Ferroelectricity in the cycloidal spiral magnetic phase of $MnWO_4$

A. H. Arkenbout,[1] T. T. M. Palstra,[1] T. Siegrist,[2] and T. Kimura[2]
[1]*Solid State Chemistry Laboratory, Materials Science Centre, University of Groningen, Nijenborgh 4, 9747 AG Groningen, The Netherlands*
[2]*Bell Laboratories, Lucent Technologies, 600 Mountain Avenue, Murray Hill, New Jersey 07974, USA*
(Received 25 July 2006; published 28 November 2006)

We investigate the relationships among magnetic, dielectric, and ferroelectric properties of a frustrated spin system $MnWO_4$, which undergoes several magnetic phase transitions including a commensurate-incommensurate and a collinear-noncollinear transition. Dielectric and pyroelectric measurements show that the transition into a spiral magnetic ordered phase produces a ferroelectric state. The direction of the electric polarization is perpendicular to the spin rotation axis and the propagation vector of the spiral. These observations agree well with recent theoretical predictions that a cycloidal spiral magnetic ordering can result in electric polarization. In a material where ferroelectricity is induced by magnetic order, we can magnetically tune the ferroelectric transitions by exploiting the difference of the net magnetization between the ferroelectric and neighboring paraelectric phases

DOI: 10.1103/PhysRevB.74.184431 PACS number(s): 75.30.Kz, 75.80.+q, 64.70.Rh

I. INTRODUCTION

Magnetoelectric multiferroics[1,2] are materials that not only show ferroelectric and magnetic order simultaneously, but also display coupling between these properties. The coupling between (ferro)electric and magnetic order is called the magnetoelectric effect and is defined as the induction of magnetization by an electric field or the induction of electric polarization by a magnetic field.[3,4] Both the magnetoelectric effect as well as multiferroics have been studied for more than four decades. However, the subject has attracted little attention, mainly because of the small value of the coupling between magnetic and ferroelectric order. In most conventional multiferroics the origin of these orders have no relation to each other. The field gained interest in recent years after the discovery of new multiferroics showing a large magnetoelectric effect, such as $TbMnO_3$,[5] $TbMn_2O_5$,[6,7] $Ni_3V_2O_8$,[8] and $CoCr_2O_4$.[9] A characteristic property of these new multiferroics is the simultaneous occurrence of a ferroelectric phase transition and a magnetic one, which suggests a strong interplay between the magnetic and ferroelectric order.

Recent theoretical studies successfully explain the mechanism of the ferroelectricity in these new multiferroics by means of both phenomenological and microscopic approaches.[8,10–13] A key factor in the ferroelectricity of these materials lies in their noncollinear spiral magnetic structures with a cycloidal component in which the magnetic structure itself breaks inversion symmetry. The general relation between electric polarization P and magnetization M in systems with spiral magnetic structures has been deduced from symmetry considerations, as described by $\vec{P} \propto \gamma \vec{e}_{ij} \times (\vec{S}_i \times \vec{S}_j)$. Here γ is a constant proportional to the spin-orbit coupling and superexchange interactions, $\vec{e}_{ij}$ is the unit vector connecting the neighboring i and j sites, and $\vec{S}$ is the magnetic moment. In this equation, $\vec{e}_{ij}$ is along the propagation vector of the spiral structure, and $(\vec{S}_i \times \vec{S}_j)$ is parallel to the spin-rotation axis. This equation indicates that a finite electric polarization can appear when the magnetic moments at sites i and j are coupled noncollinearly in a spiral manner, and the spin rotation axis is not parallel to the propagation vector. For example, the cycloidal spiral magnetic structure[14] shown in Fig. 1(a) meets these requirements. In addition, the direction of electric polarization is perpendicular to the spin rotation axis [Fig. 1(a)] and the propagation vector of spiral, and can be reversed by the change in the chirality of the spiral. The collinear sinusoidal structure $[(\vec{S}_i \times \vec{S}_j)=0$; Fig. 1(b)] as well as the screw spiral structure $[\vec{e}_{ij} \| (\vec{S}_i \times \vec{S}_j)$; Fig. 1(c)] does not induce a net polarization. Microscopically, the origin of the ferroelectricity in spiral spin systems has been reported by Katsura and co-workers.[10] The idea is that spin current (or spin chirality) is induced between noncollinear spins due to Aharonov-Casher effect[15] or an inversed effect of Dzyloshinskii-Moriya interaction.[13,16,17] These recent studies indicate that most cycloidal spiral magnets could show a multiferroic nature as well as a large magnetoelectric effect, and multiferroics should be seen in a much wider range of materials. In this paper, we examine the ferroelectric and magnetoelectric properties of another spiral magnetic

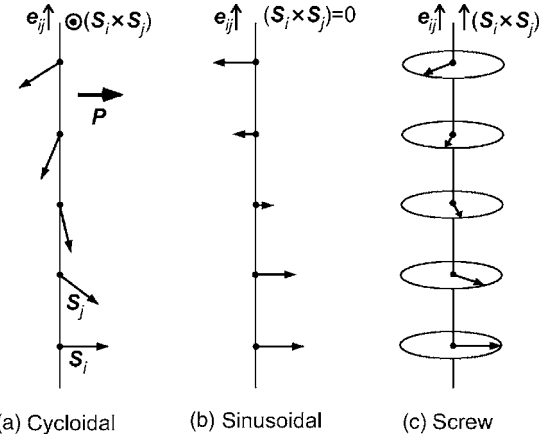

FIG. 1. Schematic illustrations of types of magnetic structure with a long wavelength. (a) Cycloidal, (b) sinusoial, and (c) screw. Geometric configurations of $\vec{e}_{ij}$ and $(\vec{S}_i \times \vec{S}_j)$ are also shown for the respective structures.

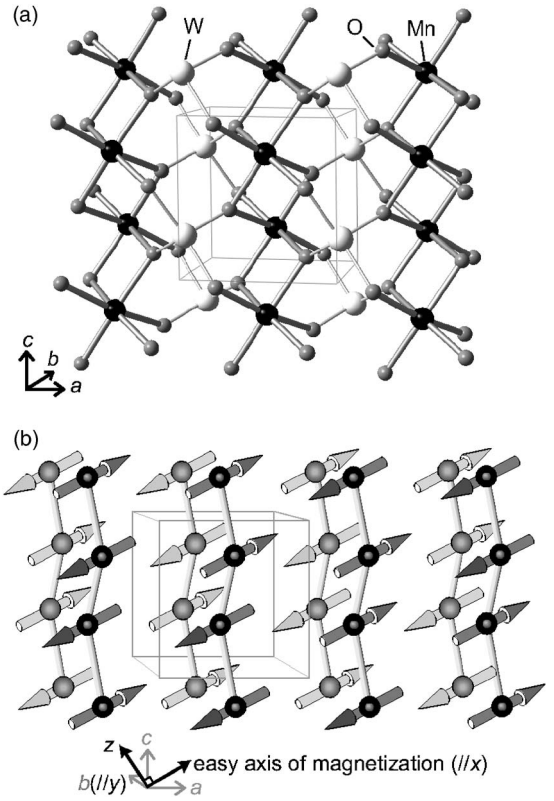

FIG. 2. (a) Crystal structure of $MnWO_4$. (b) Magnetic structure of the ground state (AF1) of $MnWO_4$. Frames indicate the crystallographic unit cell.

system, $MnWO_4$ (huebnerite), to test the theoretical prediction.

The fundamental crystal structure of $MnWO_4$ is monoclinic with space group $Pc/2$.[18,19] As shown in Fig. 2(a), the structure is composed of alternate stacking of the Mn and W layers along the a axis. Both Mn^{2+} and W^{6+} ions are coordinated by distorted octahedra of hexagonal-close-packed oxygen ions. $MnWO_4$ with magnetic Mn^{2+} is known to be a moderately frustrated antiferromagnetic (AF) system. Its Curie-Weiss constant θ is ~ -75 K, while magnetic order appears only below $T_{N3} \approx 13.5$ K. Thus the frustration parameter $f(=-\theta/T_{N3})$ is ≈ 5.[20] Below T_{N3}, there are two more magnetic transitions at $T_{N2} \approx 12.5$ K and $T_{N1} \approx 6.5-8$ K, and three magnetic ordered phases; AF1 ($T \leqslant T_{N1}$), AF2 ($T_{N1} \leqslant T \leqslant T_{N2}$), and AF3 ($T_{N2} \leqslant T \leqslant T_{N3}$) phases. In the AF1 phase below T_{N1}, the magnetic structure is commensurate with a propagation vector $\vec{k}_{AF1}=(\pm\frac{1}{4},\frac{1}{2},\frac{1}{2})$. The magnetic moments are aligned collinearly along the easy axis of magnetization, which is within the ac plane at an angle of 35°–37° from the a axis.[21,22] As illustrated in Fig. 2(b), the magnetic structure of the AF1 phase is characterized by the up-up-down-down ($\uparrow\uparrow\downarrow\downarrow$) spin configuration along both the a and the c axes, which is often realized in the ground state of the system with competing magnetic interactions.[23] In this paper, we use an orthogonal setting which differs from the crystallographic monoclinic setting to make the discussion simpler. We define the orthogonal x, y, and z axes parallel to the easy axis of magnetization, parallel to the b axis, and perpendicular to both the easy axis and the b axis, respectively [see Fig. 2(b)]. In the AF2 and AF3 phases, the propagation vector becomes incommensurate with $\vec{k}_{AF2}=(-0.214,\frac{1}{2},0.457)$. At the transition between the AF2 and AF3 phases, the incommensurate propagation vector does not change. According to the model proposed by Lautenschlager and co-workers,[22] the only difference between the two phases is the existence of a component of the magnetic moments along the $b(\|y)$ axis in the AF2 phase, which does not exist in the AF3 phase. In more detail, the magnetic structure in the AF2 phase shows an elliptically modulated noncollinear spiral spin structure, in which the basal plane of the elliptical spiral contains the easy axis of magnetization ($\|x$ axis) and the y axis. The AF3 phase is a collinear sinusoidal magnetic structure with the magnetic moments lying along the x axis. The magnetic structures of the AF2 and AF3 phases can be categorized in a cycloidal spiral as in Fig. 1(a) and a sinusoid as in Fig. 1(b), respectively. Systematic study of the magnetic, dielectric, and magnetoelectric properties of this material show various magnetic phases with collinear-noncollinear and incommensurate-commensurate transitions, which reveal that the spiral magnetic order does induce ferroelectricity.

II. EXPERIMENTAL PROCEDURES

Single crystals of $MnWO_4$ were synthesized by two different crystal growth techniques; flux growth and floating-zone (FZ) methods. In the flux growth technique, we have grown single crystals from a Na_2WO_4 flux, following Ref. 24. A mixture of $MnCO_3$, WO_3, and Na_2WO_4 powder was placed in a platinum crucible and heated up to 1250 °C. It was then slowly cooled to 600 °C at a rate of 1 °C/h. The crystals were removed from the flux by dissolving the flux material in a NaOH solution. This method resulted in dark purple crystals with typical dimensions of $\sim 2\times 2\times 2$ mm. For the FZ growth technique, first $MnWO_4$ powder was synthesized by calcination of $MnCO_3$ and WO_3 at 1050 °C for 60 h in a nitrogen gas flow. The resulting light brown powder was pressed into a rod, which was used in the floating zone setup. The rod was pulled through at a rate of 5–7 mm/h in an atmosphere of nitrogen using a halogen-lamp image furnace. The obtained crystals were as large as ~ 6 mm$\phi \times 20$ mm. The crystals could easily be cleaved perpendicular to the $b(y)$ axis, and had a transparent red-brown color. The crystals grown by both the techniques were characterized by powder and single-crystal x-ray-diffraction measurements. The powder-diffraction patterns were refined with GSAS,[25] to determine the purity of the crystals. The crystals were cut, polished, or cleaved to create the desired surfaces for the measurements of the dielectric constant and pyroelectric current. Subsequently, two electrodes were formed by sputtered gold on the widest faces of the crystals. The crystals with the gold electrodes were annealed at 400 °C for 2 h. The measurements were done in a Quantum Design physical properties measurement system (specific heat, dielectric constant, and pyroelectric current) and a Quantum Design magnetic properties measurement system (magnetization). We measured the dielectric constant at 1 MHz using an *LCR* meter. For the determination of the electric polariza-

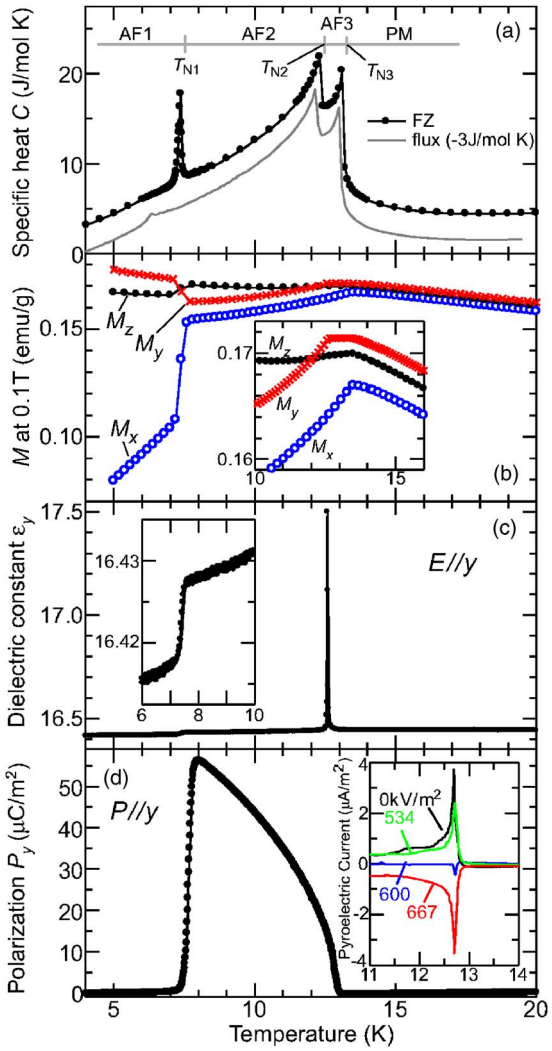

FIG. 3. (Color online) Temperature profiles of (a) specific heat, (b) magnetization (M), (c) dielectric constant along the y axis (ε_y), and (d) electric polarization along the y axis (P_y) for $MnWO_4$ crystals. The insets of (b) and (c) magnify the M around T_{N3} and the ε_y around T_{N1}, respectively. The specific data of the flux crystal in (a) are vertically offset for clear comparison. The M_x (open circles), M_y (crosses), and M_z (closed circles) in (b) were taken at a magnetic field of 0.1 T applied along the x, y, and z axes, respectively. The inset of (d) shows pyroelectric current as a function of temperature. The respective pyroelectric measurements were done in the absence of applied electric fields after a negative (or zero) electric field (E_{rev}=0, −534, −600, and −667 kV/m) is applied at 10 K (see text).

tion the sample was poled prior to every measurement to prevent for the formation of different ferroelectric domains. To this end, the sample was cooled down from the paramagnetic phase ($\geq T_{N3}$) to 2 K (at a rate of 20 K/min) in an electric field of 262 kV/m [except for the data shown in the inset of Fig. 3(d)]. Subsequently, the electric field was turned off and the current was measured while the sample was heated through the ferroelectric transition temperature at a rate of 3 K/min. The electric polarization was obtained by integrating the pyroelectric current as a function of time.

III. RESULTS AND DISCUSSION

A. Magnetic and electric properties at zero magnetic field

Powder x-ray-diffraction measurements confirmed that the crystals obtained by both growth techniques adopt the $Pc/2$ monoclinic structure at room temperature. However, the flux-grown crystals contained a few mole percent of Mn_2O_3 while no impurity phase was observed in the FZ-grown crystals. In the specific heat data it can be seen how this impurity influences the magnetic phase transitions. Figure 3(a) shows the temperature dependence of specific heat for the crystals grown by the flux and the FZ methods. Three anomalies were observed below 20 K in the specific heat for both crystals. Taking account of results of former studies,[22,26] the anomalies at 13.5 and 12.5 K are attributed to the phase transitions into the collinear sinusoidal AF3 phase at T_{N3} and the noncollinear elliptical cycloidal spiral AF2 phase at T_{N2}. The features of both transitions appear to be little affected by the quality of crystals. However, the shape and temperature of the anomaly ascribed to the transition into the AF1 phase at T_{N1} shows a remarkable difference between the flux and the FZ crystals. For the FZ crystals, a sharp peak is observed at ~7.4 K, which suggests that the transition into the AF1 phase is first order. For the flux grown crystal this transition occurs at lower temperature (~6.4 K) and becomes broader. The impurities in the flux crystal thus weaken the transition towards the AF1 phase, and stabilize this AF2 phase. This result is consistent with a neutron-diffraction study which revealed that the AF2 phase remains even at T=1.7 K in a powder sample containing impurities.[22] Therefore we will present only the data taken for the FZ-grown crystals with higher quality in the following.

Figure 3(b) displays the magnetization (M) measured at a magnetic field (H) of 0.1 T as a function of temperature. In the $M_y(T)$ three anomalies were observed at T_{N1}=7.4 K, T_{N2}=12.5 K, and T_{N3}=13.5 K. However, in $M_x(T)$ and $M_z(T)$, only two anomalies can be observed at T_{N1} and T_{N3}, and no anomaly was observed at T_{N2}. In the AF3 phase, the M_y and the M_z exhibit little temperature dependence, whereas M_x gradually decreases with decreasing temperature [see inset of Fig. 3(b)]. This indicates that the magnetic moments develop in the direction along the x axis in the AF3 phase. This is in good agreement with the neutron-diffraction result,[22] which showed that the magnetic moments are aligned along the x axis in AF3. At T_{N2}, M_y starts to decrease toward lower temperatures. In the AF2 phase ($T_{N1} \leqslant T \leqslant T_{N2}$), only M_z remains nearly constant, whereas M_x and M_y are suppressed upon cooling. Thus the transition from AF3 to AF2 involves only a change in the y component of the magnetization, and the ordered magnetic moments develop along both the x and y axes in AF2. Again, this is consistent with a former neutron result that suggested that an additional component of the moments in the direction along the y axis arises in the AF2 phase.[22] At T_{N1}, M_x decreases more rapidly, while the M_y shows a sudden increase. This can be attributed to the disappearance of the y component in M. In the AF1 phase, the magnetic moments are again aligned collinearly along the x axis.[22]

In the same temperature range as the magnetization measurements, dielectric and pyroelectric measurements have

been performed. In both measurements, an electric field was applied along the x, y, and z axes. However, significant anomalies were observed only when an electric field was applied along the y axis. Figures 3(c) and 3(d) show the temperature dependence of the dielectric constant along the y axis (ε_y) and the electric polarization along the y axis (P_y) obtained from measurements of the pyroelectric current in the absence of H.[27] At T_{N3}, no anomaly was observed in both ε_y and P_y. This indicates that the appearance of the AF3 phase with the collinear sinusoidal magnetic structure does not affect the dielectric and ferroelectric properties in $MnWO_4$. Upon cooling, ε_y exhibits a delta function at T_{N2}, which suggests the occurrence of a ferroelectric transition. In fact, a finite spontaneous polarization develops along the y axis below T_{N2}, as shown in Fig. 3(d). With further decreasing temperature, P_y increases gradually into the AF2 phase, which suggests that the transition is second order. At T_{N1} =7.4 K, a stepwise anomaly appears in ε_y, as shown in the inset of Fig. 3(c). P_y discontinuously drops at T_{N1} and disappears in the AF1 phase with the up-up-down-down spin structure.

To demonstrate switching of the spontaneous polarization by an external electric field, i.e., ferroelectricity, we performed the following experiment. First, the sample was poled by applying a positive electric field of +667 kV/m above T_{N3}, in which the sample was cooled down to 10 K. After poling, the electric field was turned off. Subsequently, a negative (or zero) electric field E_{rev} was applied, which was removed after a while. Then, pyroelectric measurements were performed in the absence of applied electric fields. The results are shown in the inset of Fig. 3(d). When $|E_{rev}|$ is less than ~600 kV/m, the sign of the pyroelectric current is not changed by the application of the negative electric field. However, the pyroelectric current is reversed when an electric field $|E_{rev}|$ was applied that was higher than ~600 kV/m. These results demonstrate that the spontaneous polarization can be reversed by an electric field and the coercive field at 10 K is around ~600 kV/m. Therefore it can be concluded that the transition into the AF2 phase leads to ferroelectric order.

The discontinuous change in the electric polarization and the shape of the anomalies in the dielectric constant and the specific heat at T_{N1} suggest that the phase transition from AF1 to AF2 is first order. This can be explained by the discontinuous change in the propagation vector of the magnetic structures.[22] The difference in the magnetic structures between AF2 and AF3 is the component of the magnetic moments in the direction of the y axis, and thus the propagation vector of both phases is the same. Therefore the T_{N2} transition is expected to be of second order, which is consistent with the present observations.

Finite electric polarization, and thus ferroelectric order, appears only in the AF2 phase where the cycloidal spiral magnetic structure has been proposed.[22] In addition, P appears in the direction along the y axis, which is perpendicular to both the spin-rotation axis ($\|z$ axis) and the propagation vector of the spiral in the proposed spin structure model by Lautenschlager and co-workers.[22] This configuration agrees completely with that predicted by recent theoretical studies,[10,12,13] which explain the appearance of ferroelectricity in systems with cycloidal spiral magnetic structures. This result indicates that the ferroelectricity in $MnWO_4$ is attributed to inversion symmetry breaking driven by the cycloidal spiral magnetic order. Conversely, the present result confirms the spin structure model proposed by the former neutron-diffraction study.

The maximum value of P_y in $MnWO_4$ is around 60 ($\mu C/m^2$), which is similar to the value of another multiferroic with a cycloidal spiral magnetic structure, $Ni_3V_2O_8$ [~100 ($\mu C/m^2$)].[8] Moreover, a similar disappearance of ferroelectricity in the ground state was also observed for $Ni_3V_2O_8$, though the crystal structures as well as the electronic configurations of magnetic ions of these two compounds are different. From the equation described in the Introduction, we anticipate a larger electric polarization in $MnWO_4$ than in $Ni_3V_2O_8$. Namely, if we only consider magnetic moments ($S=5/2$ in Mn^{2+} and $S=1/2$ in Ni^{2+}) and relative angles between $\vec{S}_i$ and $\vec{S}_j$ [~80° in $MnWO_4$ and ~50° in $Ni_3V_2O_8$], we can expect a larger P in $MnWO_4$. However, the smallness of the orbital momentum of Mn^{2+} ($L=0$) and of the y component of magnetic moments may suppress the magnitude of P in $MnWO_4$. Thus in order to obtain a large electric polarization, we need to take account of all parameters that are included in the equation.

We observed a memory effect below T_{N1}, where no substantial electric polarization could be observed. The $P(T)$ data shown in Fig. 3(d) were taken by the following poling procedure. First, the sample was cooled from above T_{N3}, while applying a poling electric field (~250 kV/m). At 2 K which is considerably below T_{N1}, the poling field was removed. Then, the pyroelectric current was measured while heating the sample. If the phase below T_{N1} is truly paraelectric, a single-domain ferroelectric state cannot be realized during the measurement after this poling procedure. However, P can be reversed completely by switching the sign of the poling electric field. In addition, the obtained $P(T)$ curve was the same as that obtained without removing the poling field during the measurement. A probable explanation for the memory effect below T_{N1} is that a small portion of the ferroelectric AF2 phase (e.g., in the form of polar nuclei) still remains below T_{N1} and preserves the polarization direction. Indeed, P did not completely disappear below T_{N1} (5–20 $\mu C/m^2$) in a polluted flux-grown crystal where the AF2 phase may remain below T_{N1} to a larger extent than that in an FZ-grown crystal (not shown). Further detailed investigations of the crystallographic and magnetic structures such as diffuse neutron-scattering study are needed to test this hypothesis.

B. Magnetic field effect on the dielectric and ferroelectric properties

Figure 4 displays the temperature dependence of ε_y and P_y in selected magnetic fields applied along the x, y, and z axes. For H along the x axis (H_x), the steplike dielectric anomaly at T_{N1} is shifted toward lower temperature with increasing H_x [Fig. 4(a)]. In agreement with the shift of ε_y, the anomaly observed at T_{N1} in P_y also decreases with increasing H_x [Fig. 4(d)]. For H_x larger than 3 T, both anoma-

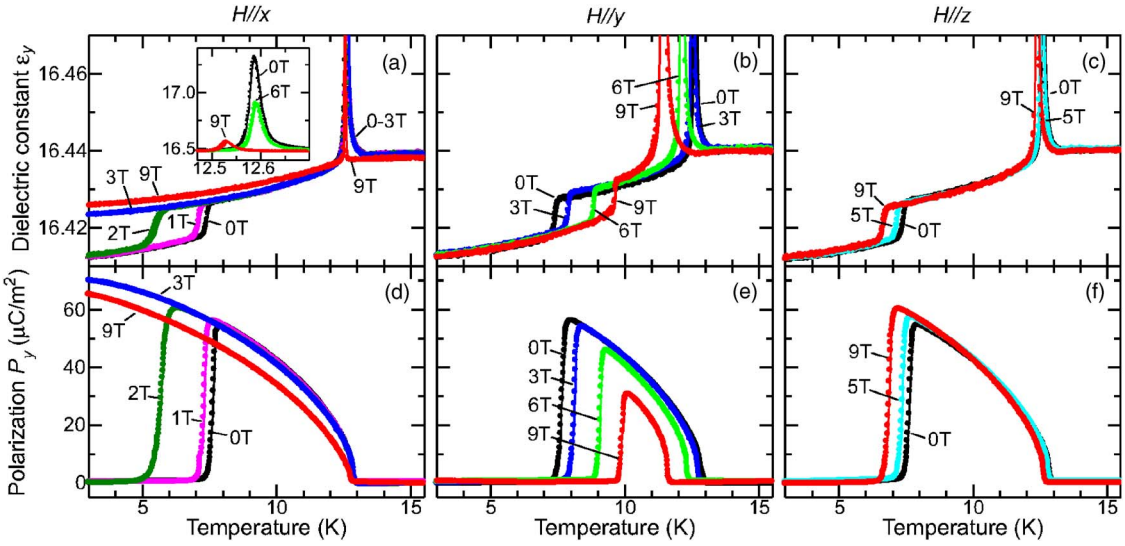

FIG. 4. (Color online) Temperature profiles of (a)–(c) dielectric constant and (d)–(f) electric polarization along the y axis at selected magnetic fields applied along the x, y, and z axes for a $MnWO_4$ crystal. The inset of (a) shows overall shapes of ε_y in the vicinity of T_{N2}.

lies in ε_y and P_y disappear down to the lowest temperature. This disappearance can be ascribed to the stabilization of the ferroelectric AF2 phase down to the lowest temperature and the suppression of the AF1 phase by H_x. Indeed, P_y at low temperature recovers in H above 3 T, as seen in Fig. 4(d). In this orientation, a finite electric polarization can be induced by a magnetic field at the lowest temperature region. It should be also noted that the divergent dielectric constant at T_{N2} is suppressed by H_x, although the peak position of ε_y at T_{N2} is slightly shifted $[dT_{N2}(9\ \mathrm{T}) \approx 0.06\ \mathrm{K}]$, as seen in the inset of Fig. 4(a). Corresponding to the suppression of the peak structure in ε_y at T_{N2}, the magnitude of P_y slightly decreases with increasing H_x above 3 T. The effect of H applied along the y axis (H_y) is distinctly different from that of H_x. As seen in Figs. 4(b) and 4(e), the anomalies in ε_y and P_y at T_{N1} are shifted toward higher temperature with increasing H_x, whereas the anomalies observed at T_{N2} shift toward lower temperature. The polarization data clearly show that the ferroelectric AF2 phase is suppressed by applying H_y. However, applying H along the z axis (H_z) affects the dielectric and ferroelectric properties less than that along x and b, as displayed in Figs. 4(c) and 4(f).

To summarize the effect of magnetic fields on the ferroelectric and magnetoelectric properties, we display the magnetic and electric phase diagrams of $MnWO_4$ for the H along the x, y, and z axes in Figs. 5(a)–5(c), respectively. The phase boundaries denoted by open triangles, crosses, and open circles were determined from anomalies in the dielectric constant, the pyroelectric current, and the specific heat. The gray areas in the phase diagrams correspond to the phase showing a finite electric polarization (or ferroelectricity). These phase diagrams are very similar to those reported by Ehrenberg and co-workers.[26] We also describe the magnetic phase boundaries obtained by our magnetization measurements as closed circles in the phase diagrams. The comparison of the electric and magnetic phase diagrams clearly demonstrates the strong interplay of the evolution of cycloidal spiral phase and ferroelectric order in $MnWO_4$.

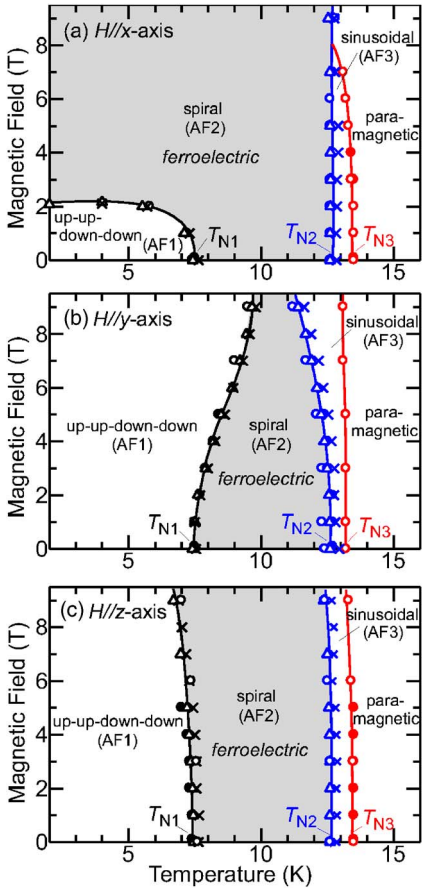

FIG. 5. (Color online) Magnetic and electric phase diagrams of $MnWO_4$ with magnetic fields applied along the (a) x, (b) y, and (c) z axes. Closed circles, open circles, open triangles, and crosses represent the data obtained by the measurements of magnetization, specific heat, dielectric constant, and pyroelectric current, respectively. Gray regions indicate ferroelectric phases.

By comparing the phase diagrams with the $M(T)$ data in Fig. 3(b), it becomes clear that the shift of the phase boundaries by H are closely related to the difference of the net magnetization between neighboring phases. When H is applied along the x axis [Fig. 5(a)], the paraelectric AF1 phase rapidly vanishes by a fairly low H ($\sim$2 T). This is related to a large jump of M_x from AF1 to AF2 [see Fig. 3(b)], which indicates that the application of H_x readily stabilizes the AF2 phase. By contrast, the high-temperature ferroelectric transition at T_{N2} is independent of the application of H_x up to 9 T. This feature is consistent with the magnetization data in which M_x is not affected by the transition at T_{N2}, as shown in the inset of Fig. 3(b). For H applied along the y axis, the ferroelectric AF2 phase shrinks while the AF1 and AF3 phases expand with increasing H_y. This variation also agrees well with the evolution of M_y which is lower in AF2 than in AF1 and AF3 [Fig. 3(b)]. As shown in Fig. 5(c), applying H along the z axis little affects the transition at T_{N2} but shifts T_{N1} slightly toward lower temperature. This can be explained also by the magnetization data: M_z at the AF1 phase is slightly smaller than that in the AF2 phase [Fig. 3(b)]. Thus we conclude that the magnetic control of ferroelectricity in $MnWO_4$ can be realized by exploiting the differences in net magnetization between the ferroelectric and neighboring paraelectric phases.

IV. CONCLUSION

We have grown high-quality single crystals of $MnWO_4$ by means of the floating zone method. Using these single crystals, we observed that $MnWO_4$ is ferroelectric only in the AF2 phase for which a cycloidal spiral magnetic structure has been proposed. In addition, the geometrical relation between the proposed magnetic structure and the direction of the electric polarization observed in the current study agrees well with the prediction of recent theoretical studies on the ferroelectricity in cycloidal spiral magnetic systems. Our study strongly suggests that $MnWO_4$ is a new member in the family of the multiferroic systems, in which the cycloidal spiral magnetic order induces a ferroelectric order. In this compound, the ferroelectric phase expands or shrinks by applying magnetic fields. The shift of phase boundaries, induced by magnetic fields, depends on the difference in the net magnetization between the ferroelectric phase and neighboring paraelectric phases. With increasing difference, the phase boundary responds stronger to applied magnetic fields. This result provides further information to design multiferroics which respond to relatively low magnetic fields. Motivated by intensive studies in the past three years, more experimental and theoretical results confirm magnetically induced ferroelectricity. However, the number of materials demonstrated experimentally is still small. Therefore our result of magnetically induced ferroelectricity in $MnWO_4$ has an important contribution in understanding and developing multiferroics research further.

Note added. Recently, the authors have learned of a similar study of the magnetoelectric study in $MnWO_4$ in a preprint server.[28] The study only focuses on the effect of magnetic fields applied along the b axis. The authors have also recently learned of another similar study.[29]

ACKNOWLEDGMENTS

We thank M. Mostovoy, F. Ye, and A. P. Ramirez for helpful discussions.

[1] H. Schmid, Ferroelectrics **62**, 317 (1994); **221**, 9 (1999).
[2] N. A. Hill, J. Phys. Chem. B **104**, 6694 (2000).
[3] H. Schmid, in *Introduction to Complex Mediums for Optics and Electromagnetics*, edited by W. S. Weiglhoger and A. Lakhtakia (SPIE Press, Bellingham, WA, 2003), p. 167.
[4] M. Fiebig, J. Phys. D **38**, R123 (2005).
[5] T. Kimura, T. Goto, H. Shintani, K. Ishizaka, T. Arima, and Y. Tokura, Nature (London) **426**, 55 (2003).
[6] K. Saito and K. Kohn, J. Phys.: Condens. Matter **7**, 2855 (1995).
[7] N. Hur, S. Park, P. A. Sharma, J. S. Ahn, S. Guha, and S-W. Cheong, Nature (London) **429**, 392 (2004).
[8] G. Lawes, A. B. Harris, T. Kimura, N. Rogado, R. J. Cava, A. Aharony, O. Entin-Wohlman, T. Yildrim, M. Kenzelmann, C. Broholm, and A. P. Ramirez, Phys. Rev. Lett. **95**, 087205 (2005).
[9] Y. Yamasaki, S. Miyasaka, Y. Kaneko, J.-P. He, T. Arima, and Y. Tokura, Phys. Rev. Lett. **96**, 207204 (2006).
[10] H. Katsura, N. Nagaosa, and A. V. Balatsky, Phys. Rev. Lett. **95**, 057205 (2005).
[11] M. Kenzelmann, A. B. Harris, S. Jonas, C. Broholm, J. Schefer, S. B. Kim, C. L. Zhang, S.-W. Cheong, O. P. Vajk, and J. W. Lynn, Phys. Rev. Lett. **95**, 087206 (2005).
[12] M. Mostovoy, Phys. Rev. Lett. **96**, 067601 (2006).
[13] I. A. Sergienko and E. Dagotto, Phys. Rev. B **73**, 094434 (2006).
[14] To express the type of spiral magnetic structures, we use the terminology (cycloidal, screw) defined by Cox *et al.* [D. E. Cox, W. J. Takei, and G. Shirane, J. Phys. Chem. Solids **24**, 405 (1963)]. If the spin-rotation axis is perpendiduclar to the propagation vector of spiral, the resulting arrangement is termed *cycloidal* structure [Fig. 1(a)]. If the spin rotation axis is parallel to the propagation vector, the arrangement gives a *screw* structure [Fig. 1(c)].
[15] Y. Aharonov and A. Casher, Phys. Rev. Lett. **53**, 319 (1984).
[16] I. Dzyloshinskii, J. Phys. Chem. Solids **4**, 241 (1958).
[17] T. Moriya, Phys. Rev. **120**, 91 (1960).
[18] H. Weitzel, Solid State Commun. **7**, 1249 (1969).
[19] A. W. Sleight, Acta Crystallogr., Sect. B: Struct. Crystallogr. Cryst. Chem. **28**, 2899 (1972).
[20] H. Dachs, Solid State Commun. **7**, 1015 (1969).
[21] H. Dachs, H. Weitzel, and E. Stoll, Solid State Commun. **4**, 473 (1966).
[22] G. Lautenschlager, H. Weitzel, T. Vogt, R. Hock, A. Bohm, M. Bonnet, and H. Fuess, Phys. Rev. B **48**, 6087 (1993).
[23] P. Bak and J. von Boehm, Phys. Rev. B **21**, 5297 (1980); P. Bak, Rep. Prog. Phys. **45**, 587 (1982).
[24] B. M. Wanklyn, J. Mater. Sci. **7**, 813 (1972).

[25] A. C. Larson and R. B. Von Dreele, General Structure Analysis System (GSAS), Los Alamos National Laboratory Report No. LAUR 86–748, 2004 (unpublished).

[26] H. Ehrenberg, H. Weitzel, C. Heid, H. Fuess, G. Wltschek, T. Kroener, J. van Tol, and M. Bonnet, J. Phys.: Condens. Matter **9**, 3189 (1997).

[27] The anomalies in P were observed at slightly higher temperatures than those in other properties such as ε. This is probably due to a higher sweeping rate of temperature (3 K/min) for measurements of the pyroelectric current, which leads to larger temperature gradient between the sample and a thermometer. Hence the transition temperature obtained by the pyroelectric measurements is slightly higher than the actual one.

[28] K. Taniguchi, N. Abe, T. Takenobu, Y. Iwasa, and T. Arima, Phys. Rev. Lett. **97**, 097203 (2006).

[29] O. Heyer, N. Hollmann, I. Klassen, S. Jpdlauk, L. Bohatý, P. Becker, J. A. Mydosh, T. Lorenz, and D. Khomskii, J. Phys.: Condens. Matter **18**, L471 (2006).